Electronic Supplementary Material (ESI) for ChemComm.

Supporting Information

Selective Targeting of PARP-1 Zinc Finger Recognition Domains With Au(III) Organometallics

Margot N. Wenzel,[a] Samuel M. Meier-Menches,[a] Thomas L. Williams,[a] Eberard Rämisch,[b] Giampaolo Barone [c] and Angela Casini[a,*]

[a] *School of Chemistry, Cardiff University, Main Building, Park Place, CF10 3AT Cardiff, United Kingdom*
[b] *Heraeus Deutschland GmbH & Co. KG, GBU Heraeus Chemicals, Heraeusstrasse 12-14, 63450 Hanau, Germany*
[c] *Dipartimento di Scienze e Tecnologie Biologiche, Chimiche e Farmaceutiche, Università di Palermo, Viale delle Scienze, Edificio 17, 90128 Palermo, Italy*

Table of contents

1. Materials

Ammonium carbonate, dimethylsulfoxide (DMSO), zinc acetate dihydrate, water (molecular biology grade), methanol (MeOH, HPLC grade) and acetonitrile (ACN, HPLC grade) were purchased from Fisher; formic acid (FA) and ubiquitin (Ub, from bovine erythrocytes) from Sigma; cytochrome C (Cyt C, from bovine heart) from Sigma Aldrich and dithiothreitol (DTT) from Alfa Aesar. All materials were used as obtained.
The zinc finger precursor peptides were obtained from Peptide Specialty Laboratories GmbH and had the sequences ^{1}PYKCPECGKSFSQKSDLVKHQRTHTG^{26} (**ZF2**) and ^{1}GRASCKKCSESIPKDSLRMAIMVQSPMFDGKVPHWYHFSCFWKV^{44} (**ZF-PARP**).
The gold(III) compounds Auphen ([Au(phen)Cl_2]PF_6 (phen = 1,10-phenantroline)),[1] Au-C^N ([Au(py^b-H)Cl_2] (py^b = 2-benzylpyridine))[2], Au-C^N^N ([Au($bipy^{dmb}$-H)(OH)]PF_6 ($bipy^{dmb}$ = 6-(1,1-dimethylbenzyl)-2,2'-bipyridine))[3] and Au-C^{a}N ([Au($phepy^a$-H)Cl_2] ($phepy^a$ = *N*-phenylpyridin-2-amine))[4] were synthesized according to literature procedures.

2. Methods

The zinc fingers were formed according to a previously published procedure.[5] In brief, the precursor peptides were incubated with DTT (3 equiv., 3 h) in ammonium carbonate buffer (25 mM, pH = 7.4) and then with zinc acetate (3 equiv., 30 min) at 37°C. The formation of the zinc fingers was assessed by a mass shift in the mass spectra. Stock solutions of the gold compounds were prepared in DMSO at a concentration of 10 mM.
The individual experiments between the gold compounds and the zinc fingers were performed at a molar ratio of 3:1 with the peptide at a final concentration of 10 µM. The compounds were typically incubated at 37°C for 5 min, but also for periods up to 24 h.
Experiments in which the drugs competed for a single peptide were carried out as Au1:Au2:Au3:Au4:ZF incubations in a molar ratio of 1:1:1:1:1. Experiments in which one complex competed for Zn-fingers or Zn-fingers plus protein (Ub/Cyt C) were carried out as Au:Zn-finger1:Zn-finger2 (:protein) incubation in a molar ratio of 3:1:1(:1).

3. Instrumentation

Samples were analysed on a Synapt G2-Si time-of-flight (TOF) mass spectrometer (Waters) by high-pressure liquid chromatography (HPLC). HPLC was performed with an Acquity UPLC system (Waters) and using an Acquity UPLC protein BEH C4 column (300 Å, 1.7 µm, 2.1 mm × 100 mm). Mass spectra were acquired and processed using MassLynx V4.1 (Waters).
The instrumental parameters for high-pressure liquid chromatography mass spectrometry (HPLC-MS) were as follows: 2.85 kV capillary voltage, 120 °C source temperature, 350 °C desolvation temperature, 90 $L \cdot h^{-1}$ cone gas, 900 $L \cdot h^{-1}$ desolvation gas and 6 bar nebulizer. A linear gradient from 95% to 5% water (0.1% FA), while proportionally increasing acetonitrile (0.1% FA), in 8 min was used to separate the peptides. The flow rate was 300 $\mu L \cdot min^{-1}$, the column was held at 40 °C and the autosampler at 20 °C.
Tandem mass spectra (ESI-MS/MS or ESI-MS^2) were acquired in a HPLC-MS setup by selecting the appropriate mass signal and fragmenting the parent ions at 18–34 eV.
Ion mobility-mass spectrometry (IM-MS) experiments were conducted on the Waters Synapt G2-Si travelling wave ion mobility instrument. The experimental settings were as follow: wave velocity 203 m/s; wave height 22.1 V; IMS DC entrance 20 V; IMS bias 3.0 V; trap gas flow 2.0 mL/min; IMS gas flow 90 mL/min; trap DC bias 45 V.

4. HPLC-ESI-MS individual experiments

a. ZF-PARP

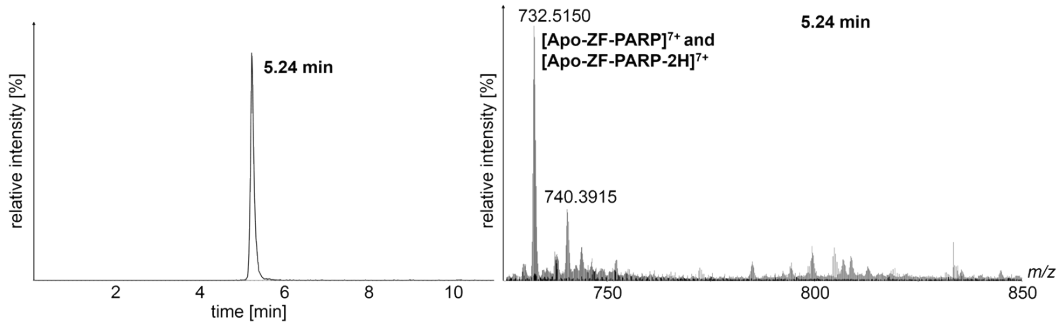

Figure S1. Chromatogram and corresponding mass spectrum of the individual HPLC-ESI-MS experiment of ZF-PARP.

Table S1. Experimental (m_{exp}) and theoretical (m_{theor}) masses of the detected species during the individual HPLC-ESI-MS experiment of ZF-PARP.

Peptide	Species	m_{exp}	M_{theor}	Δppm
ZF-PARP	$[Apo\text{-}ZF\text{-}PARP]^{7+}$	732.5150	732.5078	9.8
	$[Apo\text{-}ZF\text{-}PARP\text{-}2H]^{7+}$	732.2315	732.2188	17.3
	$[Apo\text{-}ZF\text{-}PARP+OAc\text{-}4H]^{7+}$	740.3915	740.3594	43.4

b. ZF2

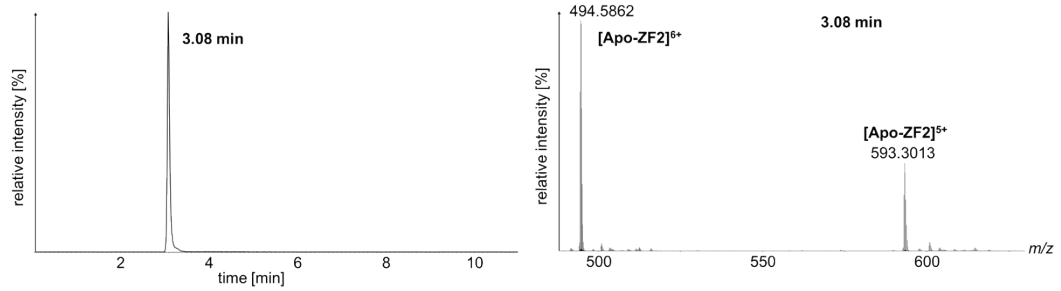

Figure S2. Chromatogram and corresponding mass spectrum of the individual HPLC-ESI-MS experiments of ZF2.

Table S2. Experimental (m_{exp}) and theoretical (m_{theor}) masses of the detected species during the individual HPLC-ESI-MS experiment of ZF2.

Peptide	Species	m_{exp}	M_{theor}	Δppm
ZF2	$[Apo\text{-}ZF2]^{6+}$	494.5862	494.5781	2.4

c. ZF-PARP and Au(III) complexes

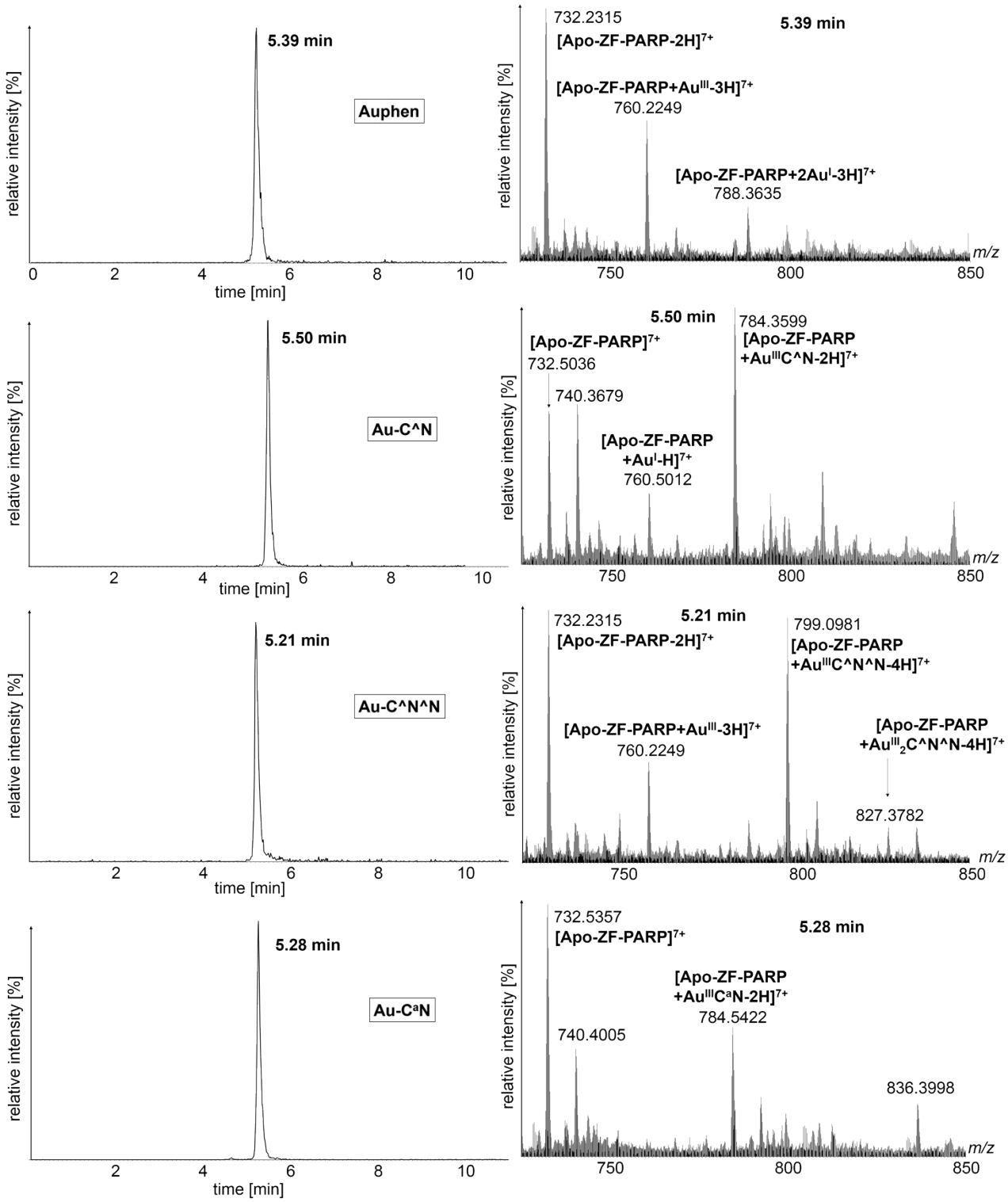

Figure S3. Chromatograms and corresponding mass spectra of the individual HPLC-ESI-MS experiments of ZF-PARP with each Au(III) complex in a 1:3 ratio for 5 min incubation at 37°C**: A.** Auphen; **B:** Au-C^N; **C:** Au-C^N^N; **D:** Au-C^{a}N.

Table S3. Experimental (m_{exp}) and theoretical (m_{theor}) masses of the detected species during the individual HPLC-ESI-MS experiments of ZF-PARP with each Au(III) complex in a 1:3 ratio for 5 min incubation at 37°C.

Compound	Species	m_{exp}	M_{theor}	Δppm
Auphen	$[Apo\text{-}ZF\text{-}PARP\text{-}2H]^{7+}$	732.2315	732.2188	17.3
	$[Apo\text{-}ZF\text{-}PARP+Au^{III}\text{-}3H]^{7+}$	760.2249	760.2109	18.4
	$[Apo\text{-}ZF\text{-}PARP+2Au^{I}\text{-}3H]^{7+}$	788.3635	788.3516	15.1
Au-C^N	$[Apo\text{-}ZF\text{-}PARP]^{7+}$	732.5036	732.5078	5.7
	$[Apo\text{-}ZF\text{-}PARP+OAc\text{-}4H]^{7+}$	740.3679	740.3594	11.5
	$[Apo\text{-}ZF\text{-}PARP+Au^{I}\text{-}H]^{7+}$	760.5012	760.5000	1.6
	$[Apo\text{-}ZF\text{-}PARP+Au^{III}C\text{^}N\text{-}2H]^{7+}$	784.3599	784.3672	9.3
Au-C^N^N	$[Apo\text{-}ZF\text{-}PARP\text{-}2H]^{7+}$	732.2315	732.2188	17.3
	$[Apo\text{-}ZF\text{-}PARP+Au^{III}\text{-}3H]^{7+}$	760.2249	760.2109	18.4
	$[Apo\text{-}ZF\text{-}PARP+Au^{III}C\text{^}N\text{^}N\text{-}4H]^{7+}$	799.0981	799.0859	15.3
	$[Apo\text{-}ZF\text{-}PARP+Au^{III}_{2}C\text{^}N\text{^}N\text{-}4H]^{7+}$	827.3782	827.3672	13.3
Au-C^{a}N	$[Apo\text{-}ZF\text{-}PARP]^{7+}$	732.5357	732.5078	38.0
	$[Apo\text{-}ZF\text{-}PARP+OAc\text{-}4H]^{7+}$	740.4005	740.3594	55.5
	$[Apo\text{-}ZF\text{-}PARP+Au^{III}C^{a}N\text{-}2H]^{7+}$	784.5422	784.5078	43.8
	$[Apo\text{-}ZF\text{-}PARP+2[Au^{III}C^{a}N\text{-}2H]]^{7+}$	836.3998	836.3672	39.0

d. ZF2 and Au(III) complexes

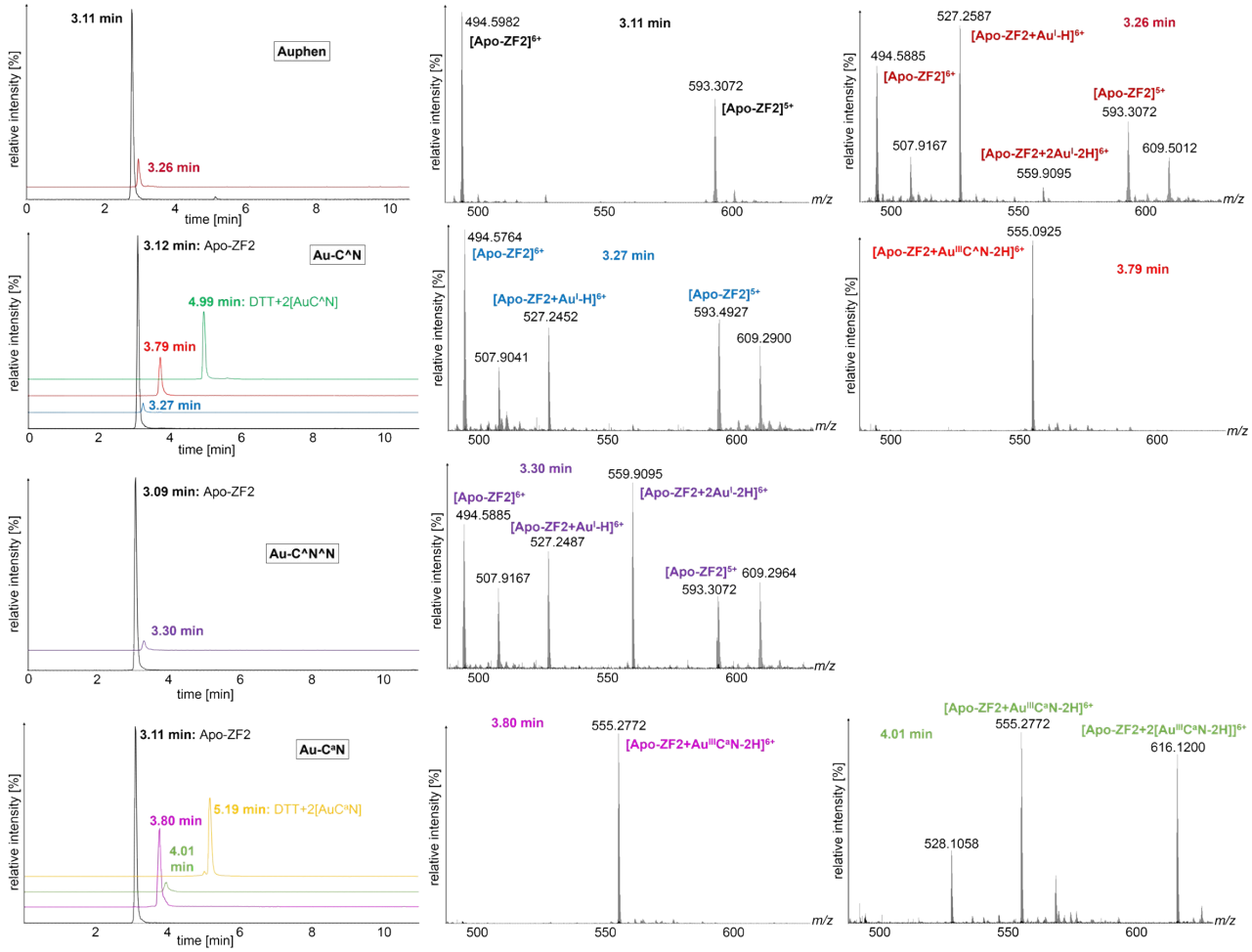

Figure S4. Chromatograms and corresponding mass spectra of the individual HPLC-ESI-MS experiments of ZF2 with each Au(III) complex in a 1:3 ratio for 5 min incubation at 37°C**: A.** Auphen; **B:** Au-C^N; **C:** Au-C^N^N; **D:** Au-C^{a}N.

Table S4. Experimental (m_{exp}) and theoretical (m_{theor}) masses of the detected species during the individual HPLC-ESI-MS experiments of ZF2 with each Au(III) complex in a 1:3 ratio for 5 min incubation at 37°C.

Compound	Species	m_{exp}	M_{theor}	Δppm
Auphen	$[Apo\text{-}ZF2]^{6+}$	494.5982	494.5781	40.6
	$[Apo\text{-}ZF2+NaOAc]^{6+}$	507.9167	507.9141	5.1
	$[Apo\text{-}ZF2+Au^{I}\text{-}H]^{6+}$	527.2587	527.2422	31.3
	$[Apo\text{-}ZF2+2Au^{I}\text{-}2H]^{6+}$	559.9095	559.8984	19.8
Au-C^N	$[Apo\text{-}ZF2]^{6+}$	494.5764	494.5781	3.4
	$[Apo\text{-}ZF2+NaOAc]^{6+}$	507.9041	507.9141	19.7
	$[Apo\text{-}ZF2+Au^{I}\text{-}H]^{6+}$	527.2452	527.2422	5.7
	$[Apo\text{-}ZF2+Au^{III}C\text{^}N\text{-}2H]^{6+}$	555.0925	555.0859	11.9
	$[DTT+2Au^{III}C\text{^}N\text{-}4H]^{+}$	881.0943	881.0859	9.5
Au-C^N^N	$[Apo\text{-}ZF2]^{6+}$	494.5885	494.5781	17.3
	$[Apo\text{-}ZF2+NaOAc]^{6+}$	507.9167	507.9141	5.1
	$[Apo\text{-}ZF2+Au^{I}\text{-}H]^{6+}$	527.2487	527.2422	18.4
	$[Apo\text{-}ZF2+2Au^{I}\text{-}2H]^{6+}$	559.9095	559.8984	19.8
Au-C^{a}N	$[Apo\text{-}ZF2]^{6+}$	494.6025	494.5781	49.3
	$[Apo\text{-}ZF2+Au^{III}C^{a}N\text{-}2H]^{6+}$	555.2772	555.2500	49.0
	$[Apo\text{-}ZF2+2[Au^{III}C^{a}N\text{-}2H]]^{6+}$	616.1200	616.0938	42.5
	$[DTT+2Au^{III}C^{a}N\text{-}4H]^{+}$	883.1203	883.0781	47.8

5. HPLC-ESI-MS competition experiments

a. Auphen + ZF2 + ZF-PARP

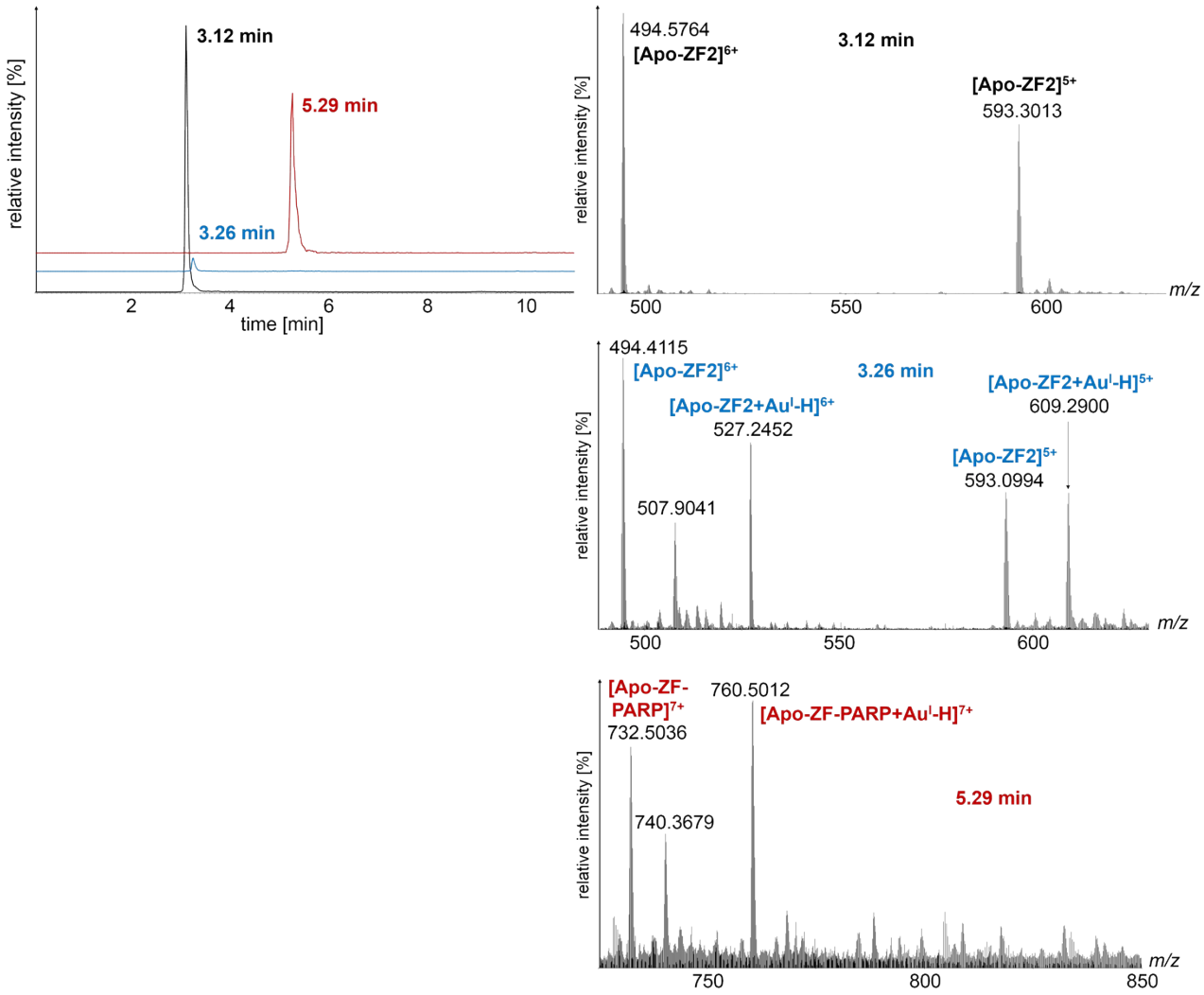

Figure S5. Extracted chromatograms and corresponding mass spectra of the competition HPLC-ESI-MS experiment of Auphen with both ZF-PARP and ZF2 in a 3:1:1 ratio for 5 min incubation at 37°C.

Table S5. Experimental (m_{exp}) and theoretical (m_{theor}) masses of the detected species during the individual HPLC-ESI-MS experiments of Auphen with both ZF-PARP and ZF2 in a 3:1:1 ratio for 5 min incubation at 37°C.

Peptide	Species	m_{exp}	M_{theor}	Δppm
ZF2	$[Apo\text{-}ZF2]^{6+}$	494.5764	494.5781	3.4
	$[Apo\text{-}ZF2+NaOAc]^{6+}$	507.9041	507.9141	19.7
	$[Apo\text{-}ZF2+Au^{I}\text{-}H]^{6+}$	527.2452	527.2422	5.7
ZF-PARP	$[Apo\text{-}ZF\text{-}PARP]^{7+}$	732.5036	732.5078	5.7
	$[Apo\text{-}ZF\text{-}PARP+OAc\text{-}4H]^{7+}$	740.3679	740.3594	11.5
	$[Apo\text{-}ZF\text{-}PARP+Au^{I}\text{-}H]^{7+}$	760.5012	760.5000	1.6

b. Au-C^N + ZF2 + ZF-PARP

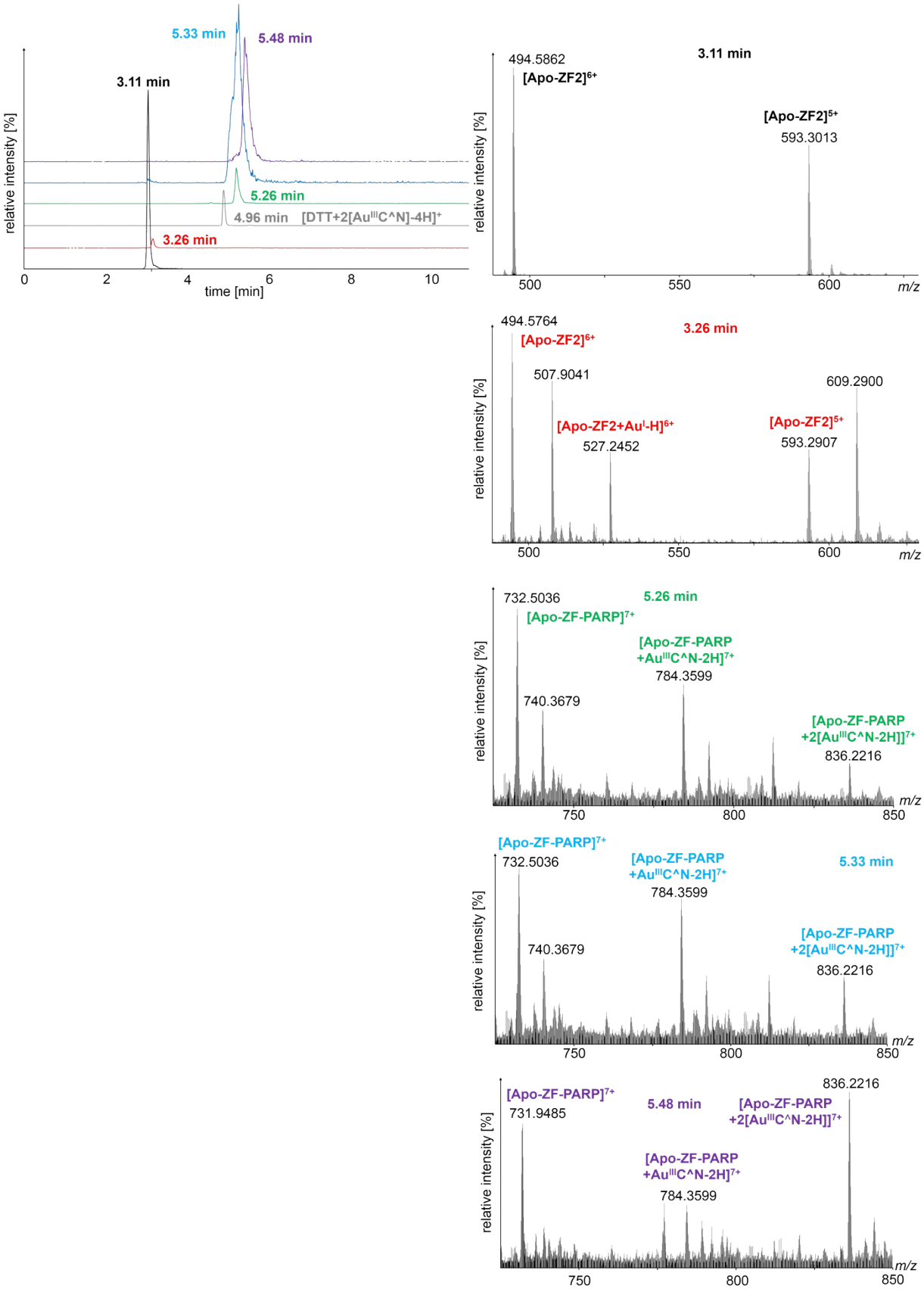

Figure S6A. Extracted chromatograms and corresponding mass spectra of the competition HPLC-ESI-MS experiment of Au-C^N with both ZF-PARP and ZF2 in a 3:1:1 ratio for 5 min incubation at 37°C.

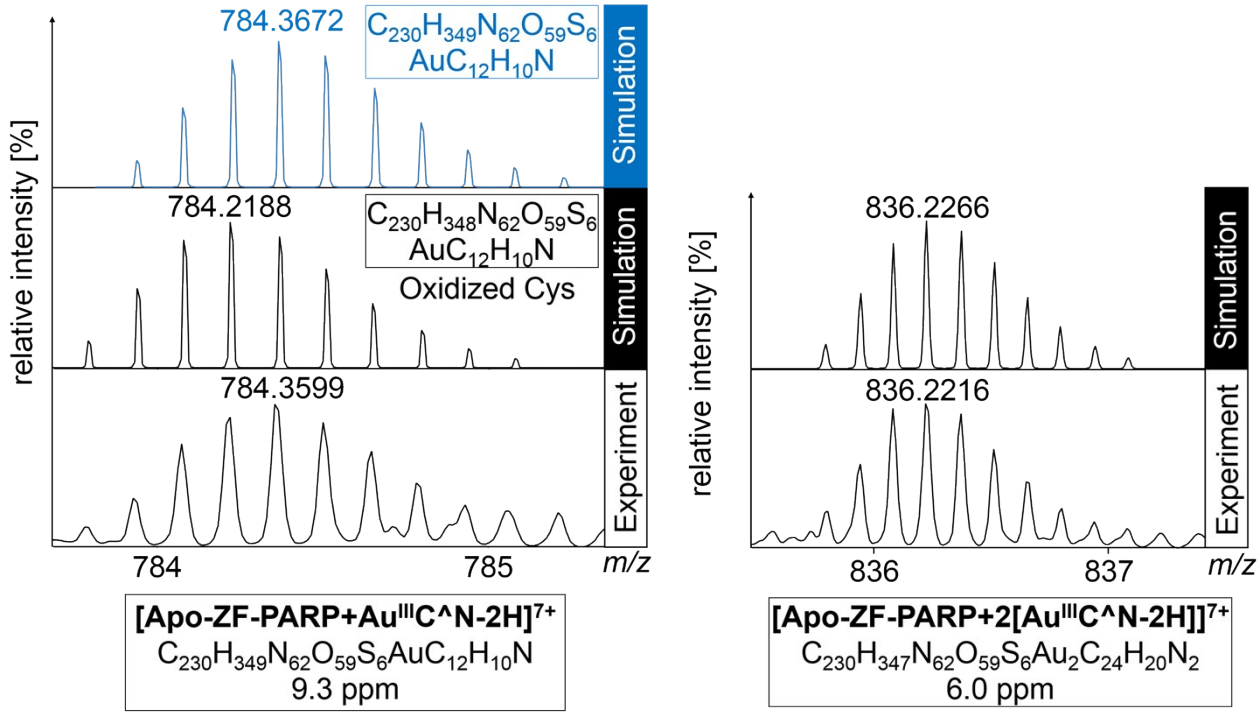

Figure S6B. Comparison between the experimental isotopic patterns of the [Apo-ZF-PARP+Au^{III}C^N-2H]$^{7+}$ and the [Apo-ZF-PARP+2[Au^{III}C^N-2H]]$^{7+}$ adducts with the theoretical values.

Table S6. Experimental (m_{exp}) and theoretical (m_{theor}) masses of the detected species during the individual HPLC-ESI-MS experiments of Au-C^N with both ZF-PARP and ZF2 in a 3:1:1 ratio for 5 min incubation at 37°C.

Peptide	Species	m_{exp}	M_{theor}	Δppm
ZF2	[Apo-ZF2]$^{6+}$	494.5862	494.5781	16.4
	[Apo-ZF2+NaOAc]$^{6+}$	507.9041	507.9141	19.7
	[Apo-ZF2+Au^{I}-H]$^{6+}$	527.2452	527.2422	5.7
-	[DTT+2[Au^{III}C^N]-4H]$^{+}$	881.1094	881.1094	0
ZF-PARP	[Apo-ZF-PARP]$^{7+}$	732.5036	732.5078	5.3
	[Apo-ZF-PARP+OAc-4H]$^{7+}$	740.3679	740.3594	11.5
	[Apo-ZF-PARP+Au^{III}C^N-2H]$^{7+}$	784.3599	784.3672	9.3
	[Apo-ZF-PARP+2[Au^{III}C^N-2H]]$^{7+}$	836.2216	836.2266	6.0

c. Au-C$^{\alpha}$N + ZF2 + ZF-PARP

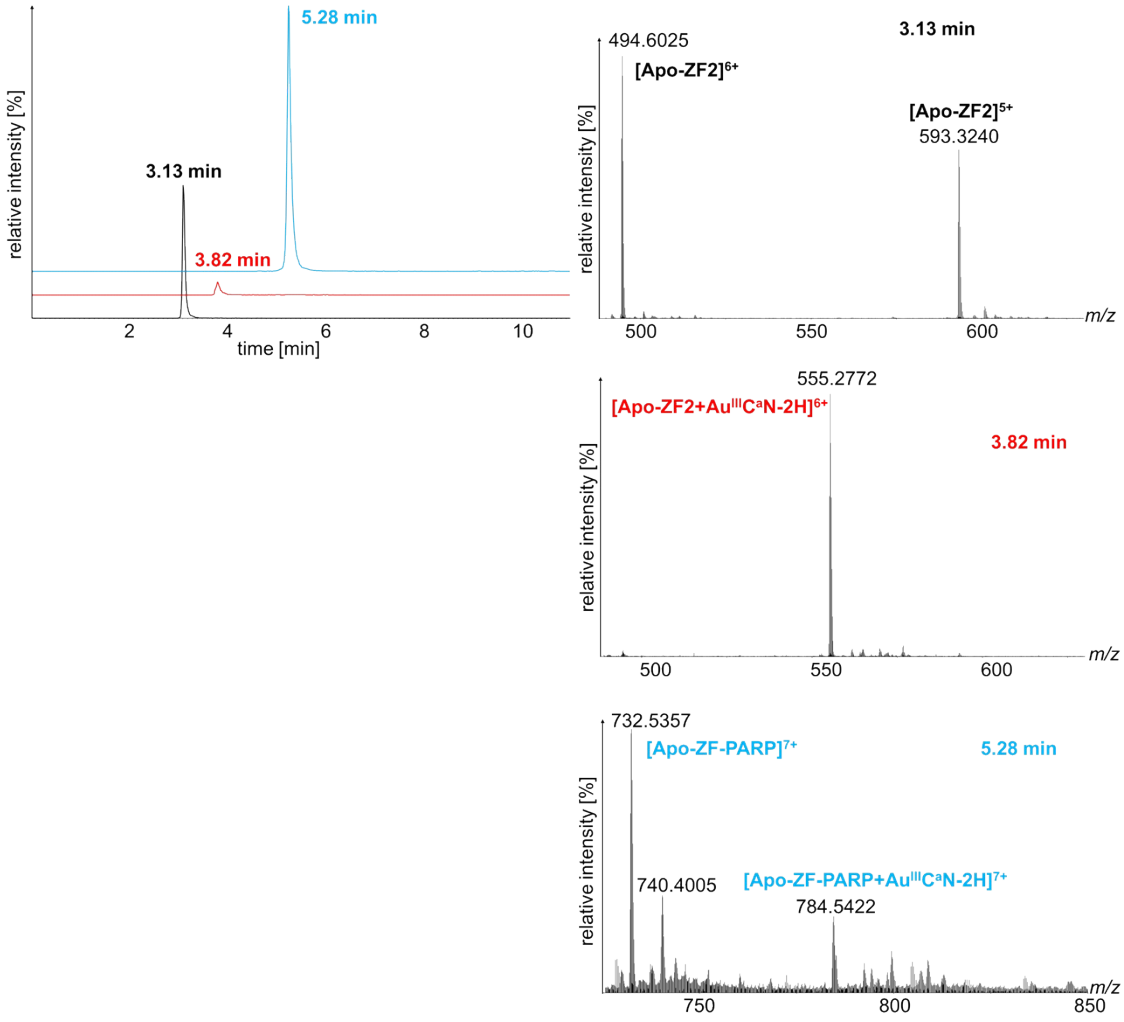

Figure S7. Extracted chromatograms and corresponding mass spectra of the competition HPLC-ESI-MS experiment of Au-C^{a}N with both ZF-PARP and ZF2 in a 3:1:1 ratio for 5 min incubation at 37°C.

Table S7. Experimental (m_{exp}) and theoretical (m_{theor}) masses of the detected species during the individual HPLC-ESI-MS experiments of Au-C^{a}N with both ZF-PARP and ZF2 in a 3:1:1 ratio for 5 min incubation at 37°C.

Peptide	Species	m_{exp}	M_{theor}	Δppm
ZF2	[Apo-ZF2]$^{6+}$	494.6025	494.5781	49.3
	[Apo-ZF2+Au^{III}C^{a}N-2H]$^{6+}$	555.2772	555.2500	49.0
ZF-PARP	[Apo-ZF-PARP]$^{7+}$	732.5357	732.5078	38.1
	[Apo-ZF-PARP+OAc-4H]$^{7+}$	740.4005	740.3594	55.5
	[Apo-ZF-PARP+ Au^{III}C^{a}N-2H]$^{7+}$	784.5422	784.5078	43.8

d. Au-C^N^N + ZF2 + ZF-PARP

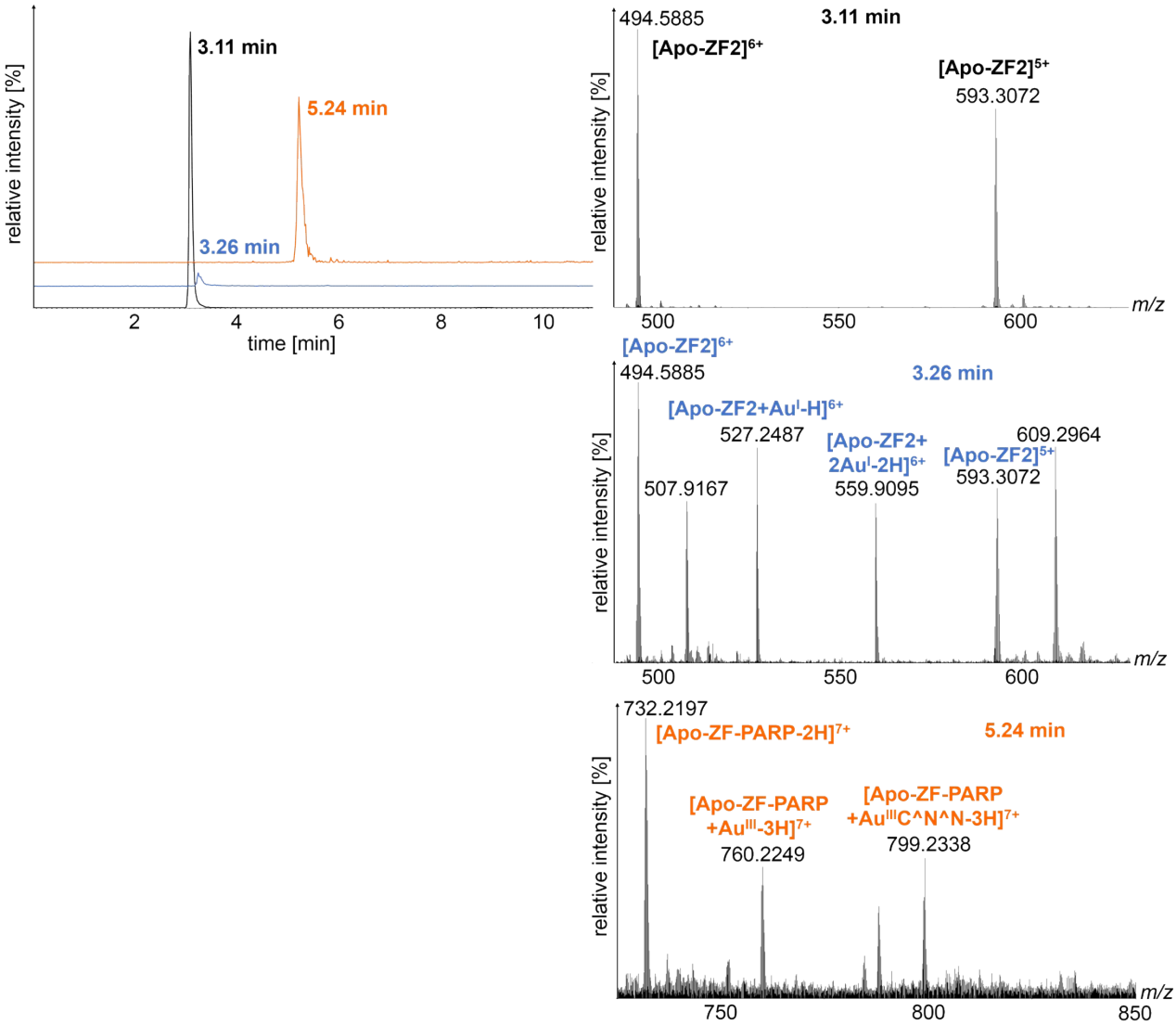

Figure S8. Extracted chromatograms and corresponding mass spectra of the competition HPLC-ESI-MS experiment of Au-C^N^N with both ZF-PARP and ZF2 in a 3:1:1 ratio for 5 min incubation at 37°C.

Table S8. Experimental (m_{exp}) and theoretical (m_{theor}) masses of the detected species during the individual HPLC-ESI-MS experiments of Au-C^N^N with both ZF-PARP and ZF2 in a 3:1:1 ratio for 5 min incubation at 37°C.

Peptide	Species	m_{exp}	M_{theor}	Δppm
ZF2	$[Apo\text{-}ZF2]^{6+}$	494.5885	494.5781	21.0
	$[Apo\text{-}ZF2+NaOAc]^{6+}$	507.9167	507.9141	5.1
	$[Apo\text{-}ZF2+Au^{I}\text{-}H]^{6+}$	527.2487	527.2422	12.3
	$[Apo\text{-}ZF2+2Au^{I}\text{-}2H]^{6+}$	559.9095	559.8984	19.8
ZF-PARP	$[Apo\text{-}ZF\text{-}PARP\text{-}2H]^{7+}$	732.2197	732.2188	1.2
	$[Apo\text{-}ZF\text{-}PARP+Au^{III}\text{-}3H]^{7+}$	760.2249	760.2109	18.4
	$[Apo\text{-}ZF\text{-}PARP+Au^{III}C\text{^}N\text{^}N\text{-}3H]]^{7+}$	799.2338	799.2344	0.8

e. Auphen + ZF-PARP + Cyt C

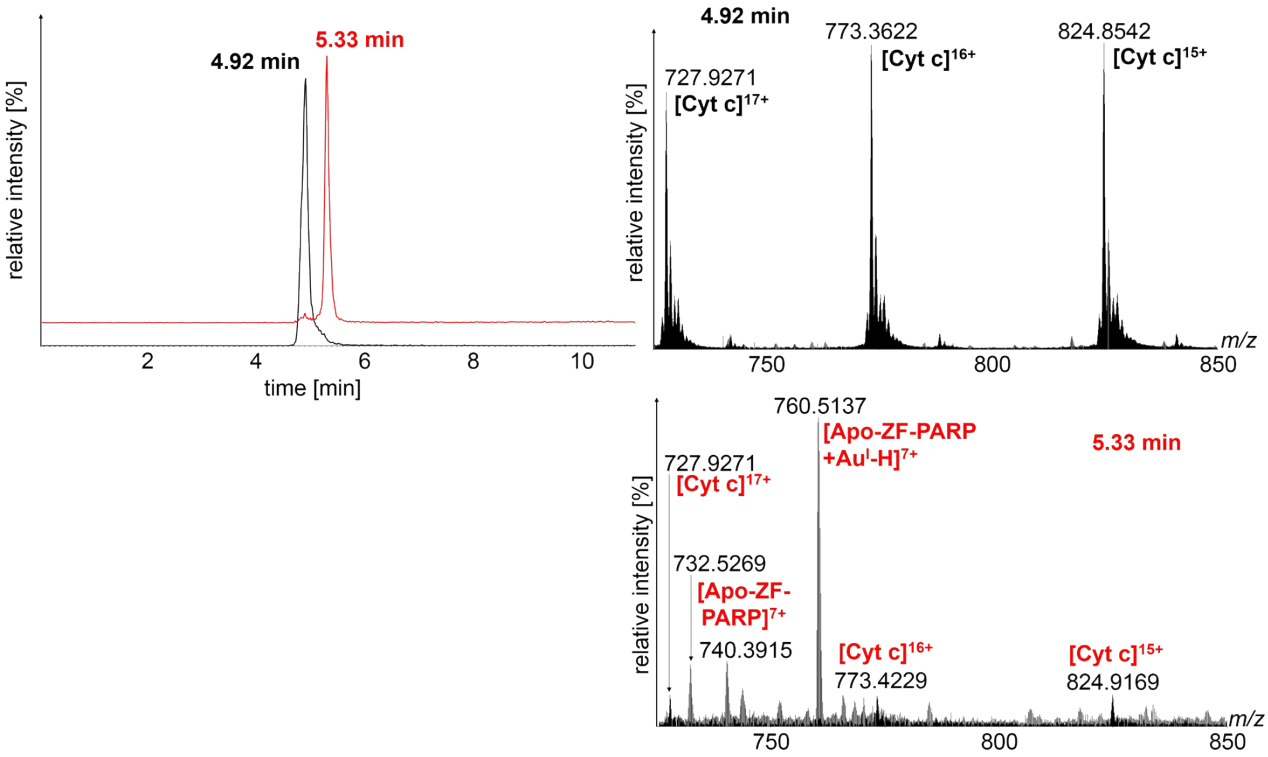

Figure S9. Extracted chromatograms and corresponding mass spectra of the competition HPLC-ESI-MS experiment of Auphen with both ZF-PARP and cyt c in a 3:1:1 ratio for 5 min incubation at 37°C.

Table S9. Experimental (m_{exp}) and theoretical (m_{theor}) masses of the detected species during the individual HPLC-ESI-MS experiments of Auphen with both ZF-PARP and cyt c in a 3:1:1 ratio for 5 min incubation at 37°C.

Peptide	Species	m_{exp}	M_{theor}	Δppm
Cyt c	$[Cyt\ c]^{17+}$	824.8542	824.8984	53.6
ZF-PARP	$[Apo\text{-}ZF\text{-}PARP]^{7+}$	732.5269	732.5078	26.1
	$[Apo\text{-}ZF\text{-}PARP+OAc\text{-}4H]^{7+}$	740.3915	740.3594	43.4
	$[Apo\text{-}ZF\text{-}PARP+ Au^{I}\text{-}H]^{7+}$	760.5137	760.5000	18.0

f. Au-C^N + ZF-PARP + Cyt c

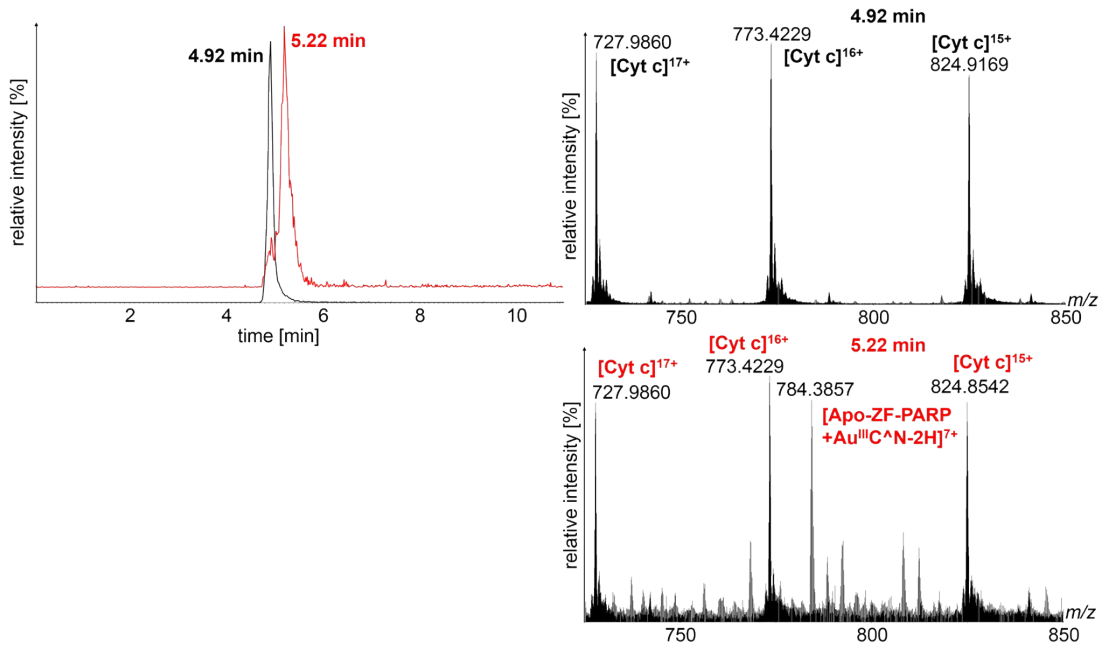

Figure S10. Extracted chromatograms and corresponding mass spectra of the competition HPLC-ESI-MS experiment of Au-C^N with both ZF-PARP and cyt c in a 3:1:1 ratio for 5 min incubation at 37°C.

Table S10. Experimental (m_{exp}) and theoretical (m_{theor}) masses of the detected species during the individual HPLC-ESI-MS experiments of Au-C^N with both ZF-PARP and cyt c in a 3:1:1 ratio for 5 min incubation at 37°C.

Peptide	Species	m_{exp}	M_{theor}	Δppm
Cyt c	$[Cyt\ c]^{16+}$	773.4229	773.4063	21.4
ZF-PARP	$[Apo\text{-}ZF\text{-}PARP+\ Au^{III}C\text{^}N\text{-}2H]^{7+}$	784.3857	784.3672	23.6

6. Binding Preference Ratio (BPR) calculation

Calculating the binding preference towards ZF-PARP over ZF2 is based on the assumption that the ionization efficiency of each gold-adduct is similar to the corresponding unreacted ZF peptide because zinc is replace by gold in the ZF structure. Percentages for forming gold-adducts are obtained for ZF-PARP and ZF2 separately by summing up the attributable peak areas obtained from the extracted ion chromatograms (EIC) of each unreacted ZF-domain and the respective interaction products. Those percentages are then expressed as a ratio (binding preference ratio, BPR).

$$\%ZF2 = \frac{A(Au-adducts, z=6+)}{A(unreacted\ ZF2, z=6+) + A(Au-adducts, z=6+)}$$

%ZF2 is the percentage of ZF2 involved in forming adducts with gold. A(x) denotes the area of the extracted ion chromatogram corresponding to the ZF2 species in charge state z = 6+.

$$\%ZF-PARP = \frac{A(Au-adducts, z=7+)}{A(unreacted\ ZF-PARP, z=7+) + A(Au-adducts, z=7+)}$$

%ZF-PARP is the percentage of ZF-PARP involved in forming adducts with gold. A(x) denotes the area of the extracted ion chromatogram corresponding to the ZF-PARP species in charge state z = 7+.

$$BPR = \frac{\%ZF - PARP}{\%ZF2}$$

The binding preference (BPR) is given as the ratio of the two percentages for forming gold-adducts.

Table S11. Peak areas data obtained from the competition experiments between the two types of ZFs and Auphen, Au-C^N, Au-C^N^N and Au-C^{a}N and calculations of the BPR for each gold complex.

	Areas of the extracted ion chromatogram (corresponding m/z)			
	Auphen	**Au-C^N**	**Au-C^N^N**	**Au-C^{a}N**
Peak area for unreacted ZF2	159819.23 (494.58)	245979.3 (494.58)	108725.02 (494.60)	137075.41 (494.60)
Peak areas for gold-ZF2 adducts	3121.96 (527.25)	5060.35 (527.25)	2579.46 (527.25)	15748.48 (555.28)
			1763.99 (559.91)	
Summed areas for gold-ZF2 adducts	3121.96	5060.35	4343.45	15748.48
Peak area for unreacted ZF-PARP	10812.22 (732.50)	13031.05 (732.50)	2624.89 (732.22)	80279.73 (732.54)
Peak areas for gold-ZF-PARP adducts	13377.21 (760.50)	13316.33 (784.36)	1148.48 (760.22)	19820.05 (784.54)
		9675.62 (836.22)	481.01 (799.23)	
Summed areas for gold-ZF-PARP adducts	13377.21	22991.95	1629.49	19820.05
%ZF2	0.01916	0.02016	0.03841	0.10305
%ZF-PARP	0.55302	0.63826	0.38301	0.19800
BPR	**29**	**32**	**10**	**2**

7. Fragmentation experiments

(A)

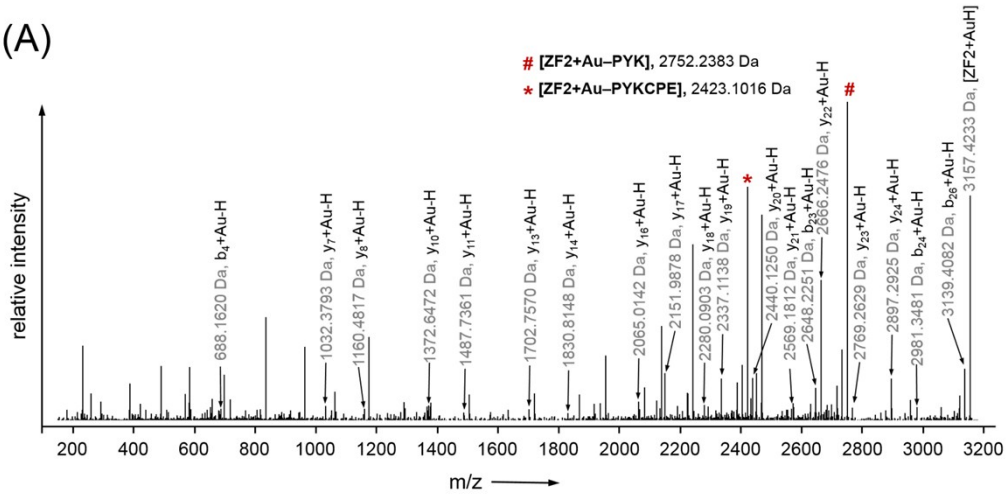

(B)

Compound	Adduct	m/z	Identified metallated fragments
Auphen	ZF2 + Au(I)	527.25	P Y K C P E C G K S F S Q K S D L V K H Q R T H T G
Au(C^N)	ZF2 + Au(C^N)	555.26	P Y K C P E C G K S F S Q K S D L V K H Q R T H T G

(C)

Compound	Adduct	m/z	Identified metallated fragments
Auphen	ZF-PARP + Au(III)	760.50	G R A S C K K C S E S I P K D S L R M A I M V Q S P M F D G K V P H W Y H F S C F W K V
Au(C^N)	ZF-PARP + Au(C^N)	784.50	G R A S C K K C S E S I P K D S L R M A I M V Q S P M F D G K V P H W Y H F S C F W K V

Figure S11. (**A**) Example of a deconvoluted fragment-mass spectrum of the adduct ZF2+Au(I) from the interaction between individual ZF2 and Auphen. (**B**) List of the different metallated b- and y-fragments for two adducts from the reactions of individual ZF2 with Auphen and Au(C^N), respectively. (**C**) List of the different metallated b- and y-fragments for two respective adducts from the competitive reactions of ZF2/ZF-PARP with Auphen and Au(C^N), respectively.

8. Ion mobility mass spectrometry experiments

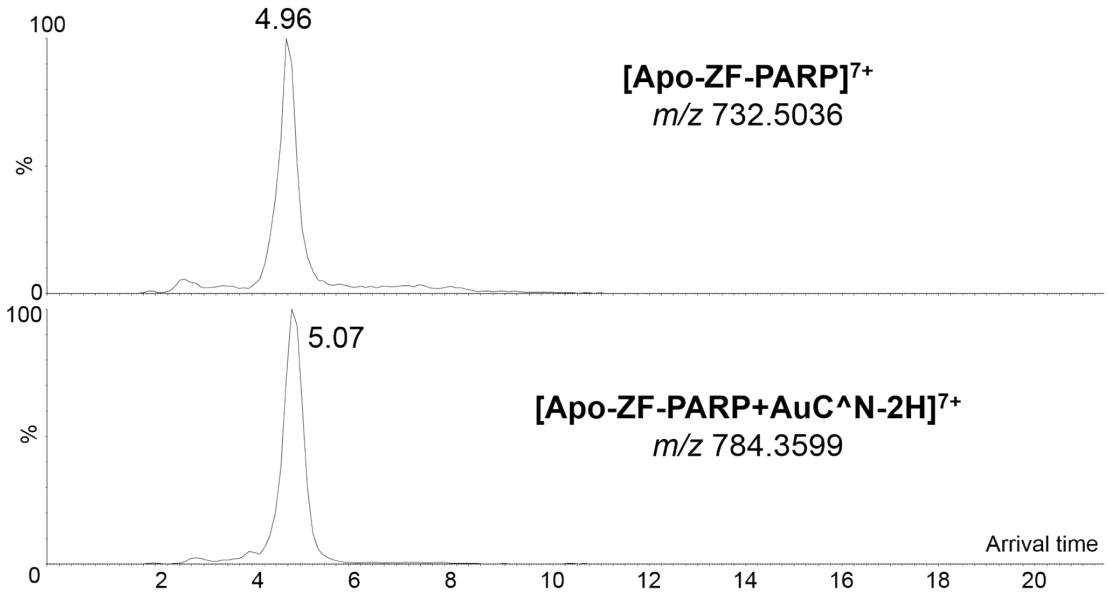

Figure S12. Extracted arrival time distributions (ms) of Apo-ZF-PARP and Apo-ZF-PARP+Au-C^N-2H.

9. Computational studies

DFT and QM/MM calculations: DFT calculations were performed by following recently reported procedures,[6] on the structures of **Au-C^N**, **Au-C^{a}N** and **Au-C^N^N**, of cysteinato, histidine and Cl^- ligands, as well as of the adducts obtained by substituting one or two chlorido ligands with cysteinato and/or histidine ligands (see Figures S13-S16). The M06-L[7] DFT functional, the Lanl2dz[8] basis set for Au, S and Cl atoms and the 6-31G(d,p)[9] basis set for C, N, O and H atoms were used. Solvent effects were evaluated by full geometry optimization within the implicit water solvent, reproduced by the polarizable continuum model (PCM).[10] Vibration frequency calculations, within the harmonic approximation, were performed to confirm that each optimized geometry corresponded to a minimum in the potential energy surface, and to evaluate the standard Gibbs free energy values, at 298.15 K, of each energy minimum structure.
QM/MM calculations have been performed to mimic the binding of **Au-C^N** with two cysteinato residues of the zinc-finger domain of PARP-1 (PDB ID: 2DMJ). The PDB file 2DMJ contains 20 protein conformations, resolved by NMR, in which the zinc coordination site is almost perfectly the same in all conformations. The first structure was selected for the QM/MM calculations and its geometry was fully optimized. The M06-L DFT functional was used in the QM layer (atoms in balls and sticks in Figure S17), composed by the Cys5, Cys8, His37 and Cys40 residues of the protein (see Figure 1b) and by the gold(III) complex. The UFF force field[11] was used in the MM layer (atoms in wires in Figure S17). Full geometry optimization was followed by a frequency analysis, to confirm that the obtained structure corresponded to an energy minimum in the potential energy surface. All calculations were performed by the Gaussian 09 program package.[12]

Results and discussion: The main aim of the DFT study was to calculate the binding strength of **Au-C^N**, **Au-C^{a}N** and **Au-C^N^N** with the Cys and His residues coordinating the Zn(II) ion in the zinc finger domain of PARP-1. The structures of the histidine and cysteinato adducts, obtained after full geometry optimization, are shown in Figures S13-S16.

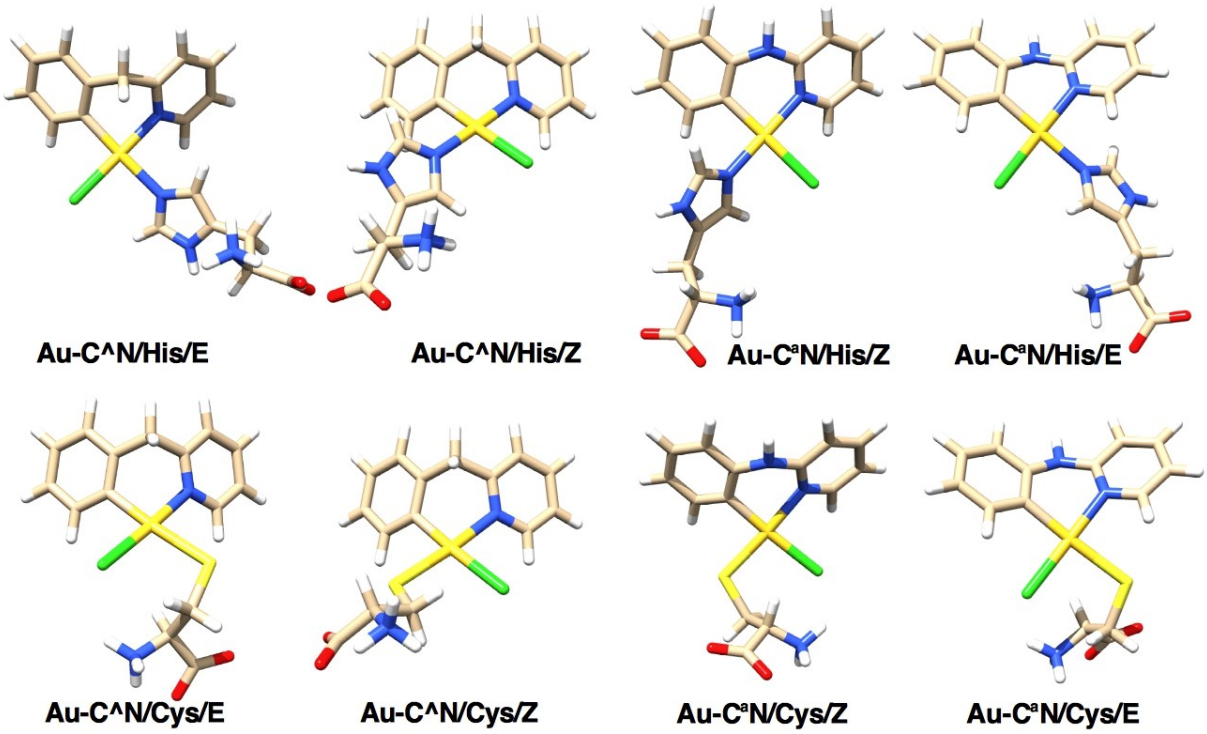

Figure S13. Structure of **Au-C^N** and **Au-C^{a}N** complexes with one cysteinato or histidine ligand, obtained by DFT calculations.

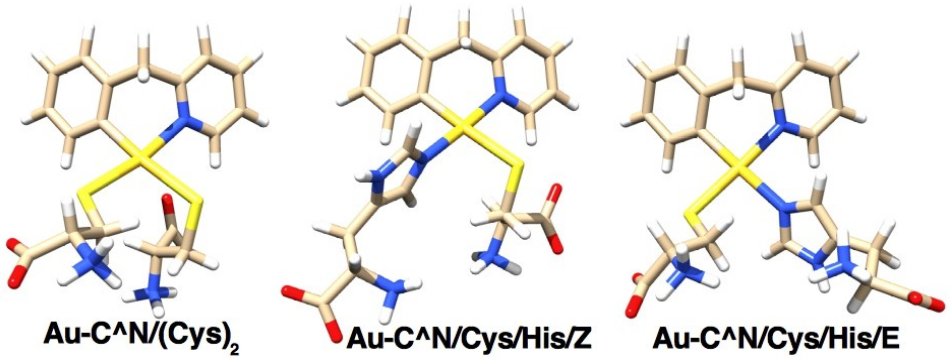

Figure S14. Structure of **Au-C^N** complex with two cysteinato or mixed cysteinato-histidine ligands, obtained by DFT calculations.

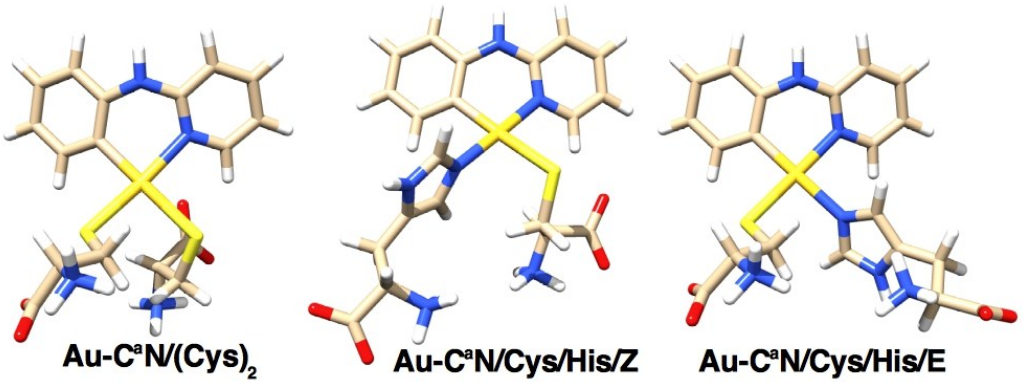

Figure S15. Structure of **Au-C^{a}N** complex with two cysteinato or mixed cysteinato-ligands, obtained by DFT calculations.

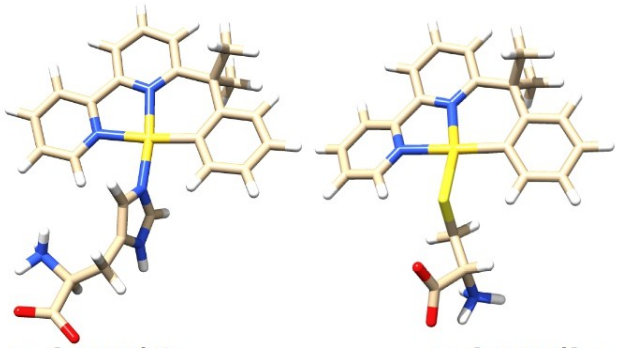

Figure S16. Structure of **Au-C^N^N** complex with one cysteinato or histidine ligand, obtained by DFT calculations.

The standard Gibbs formation free energy values of the gold compounds-amino acid adducts, reported in Table S12, were obtained by hypothesizing the occurrence of the following reactions:

$[Au(Ligand)Cl]^{n+} + Cys^- \rightarrow [Au(Ligand)Cys]^{n+} + Cl^-$
$[Au(Ligand)Cl]^{n+} + His \rightarrow [Au(Ligand)His]^{(n+1)+} + Cl^-$
$[Au(Ligand)Cl_2]^{n+} + 2Cys^- \rightarrow [Au(Ligand)(Cys)_2]^{n+} + 2Cl^-$
$[Au(Ligand)Cl_2]^{n+} + Cys^- + His \rightarrow [Au(Ligand)CysHis]^{(n+1)+} + 2Cl^-$

where n is the charge of the metal complex, and calculated by the Eqn. 1-4 below, where G° is the standard Gibbs free energy in solution:

$\Delta G° = G°[Au(Ligand)Cys] + G°[Cl^-] - G°[Au(Ligand)Cl] - G°[Cys^-]$ Eq. 1
$\Delta G° = G°[Au(Ligand)His] + G°[Cl^-] - G°[Au(Ligand)Cl] - G°[His]$ Eq. 2
$\Delta G° = G°[Au(Ligand)(Cys)_2] + 2\ G°[Cl^-] - G°[Au(Ligand)Cl_2] - 2\ G°[Cys^-]$ Eq. 3
$\Delta G° = G°[Au(Ligand)(Cys)(His)] + 2\ G°[Cl^-] - G°[Au(Ligand)Cl_2] - G°[His] - G°[HCys]$ Eq. 4

Table S12. Standard Gibbs formation free energy in water solution, ΔG° in kJ/mol, of the adducts of **Au-C^N**, **Au-C^{a}N** and **Au-C^N^N** with Cys and His ligands, obtained by DFT calculations and using Eqs. 1-4.

Au-C^N / Cys / E	-37.7	**Au-C^N / His / E**	46.5
Au-C^N / Cys / Z	-82.5	**Au-C^N / His / Z**	37.5
Au-C^N / $(Cys)_2$	-132.9		
Au-C^{a}N / Cys / E	-37.2	**Au-C^{a}N / His / E**	43.5
Au-C^{a}N /Cys/Z	-90.1	**Au-C^{a}N / His / Z**	34.5
Au-C^{a}N /$(Cys)_2$	-128.4		
Au-C^N^N / Cys	-70.8	**Au-C^N^N / His**	52.9
Au-C^N / Cys / His / Z	7.7		
Au-C^N / Cys / His / E	-32.4		
Au-C^{a}N / Cys / His / E	-32.0		
Au-C^{a}N / Cys / His / Z	3.1		

The results obtained show that the binding with histidine always provides positive formation energy values and indicate that such complexes are less stable than the starting chloro complexes. On the other hand, the results show that the binding with one or two cysteinato ligands stabilizes the product. Particularly interesting is the binding of **Au-C^N** with two cysteinato ligands, because the formation energy of such adduct (-132.9 kJ/mol) is greater than the sum of the formation energy obtained by the binding with one cysteinato ligand, in the two E and Z isomers, after replacing only one chlorido ligand (-37.7 and -82.5 kJ/mol). Moreover, the results show that the binding with two cysteinato is highly favored also compared to the mixed binding with one cysteinato and one histidine ligands. Finally, the binding of **Au-C^N** with two cysteinato ligands is slightly favored compared to the analogous binding with **Au-C^{a}N**.

For this reason, QM/MM calculations have been performed on the structures obtained by the PDB 2DMJ file, removing the Zn(II) ion and adding the **Au-C^N** complex, without the two chlorido ligands, coordinated by the Cys40 and Cys8 residues. The latter residues are the most external groups in the zinc-finger cavity, as shown by the structures obtained after full geometry optimization (Figure S16). The remaining Cys5 residue was protonated before performing the QM/MM calculations, considering the physiological pH of the experimental conditions.

As shown in Figure S17, four different isomers can be obtained by changing the orientation of the approaching Au(III) compound and considering the isomerism around the CH_2 bridge of the **C^N** ligand. The SCF energy calculated for the QM layer shows that the three of the four isomers have essentially the same stability. Superimposing the four optimized structures (Figure S18), it is also possible to see that the four binding isomers induce a similar overall distortion in the protein. Finally, superimposing the structure of the most stable isomer with that of the original PDB 2DMJ file, optimized at the same level of theory, it can be observed that the overall protein folding is essentially preserved (Figure S19).

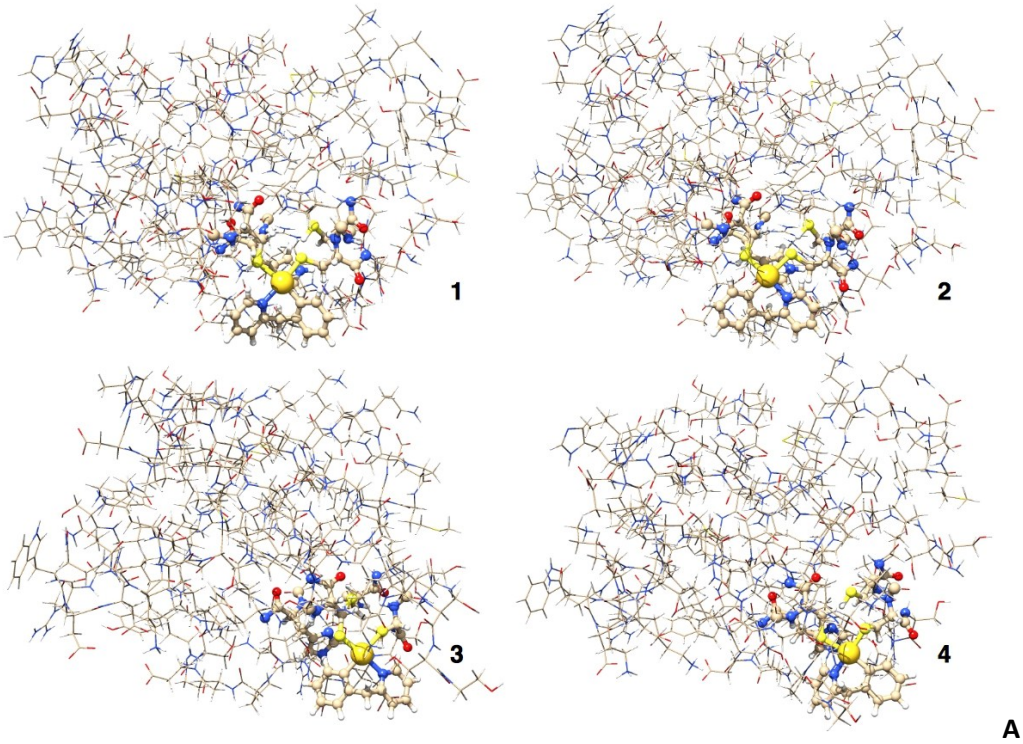

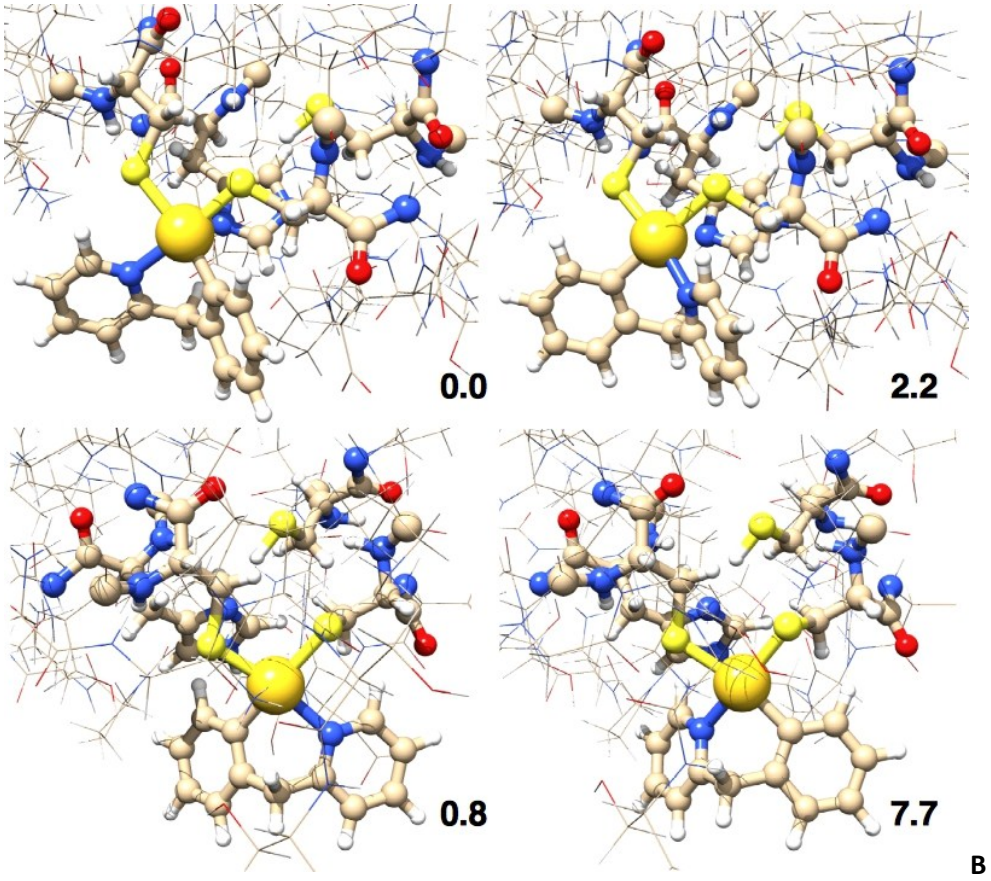

Figure S17. Structure of four isomers found to mimic the possible binding of Au-C^N with the zinc finger domain of PARP-1. **A)** whole system; **B)** expanded region around the higher QM layer, showing also the relative SCF energy (in kJ/mol). QM layer represented as balls and sticks, MM layer as wires.

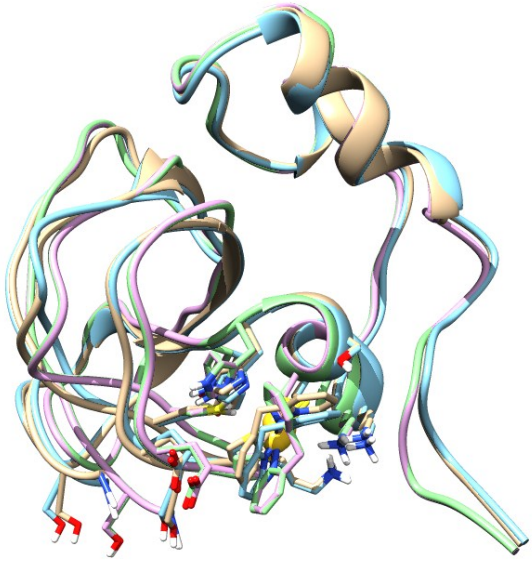

Figure S18. Superimposed structures of the four isomers found by QM/MM calculations.

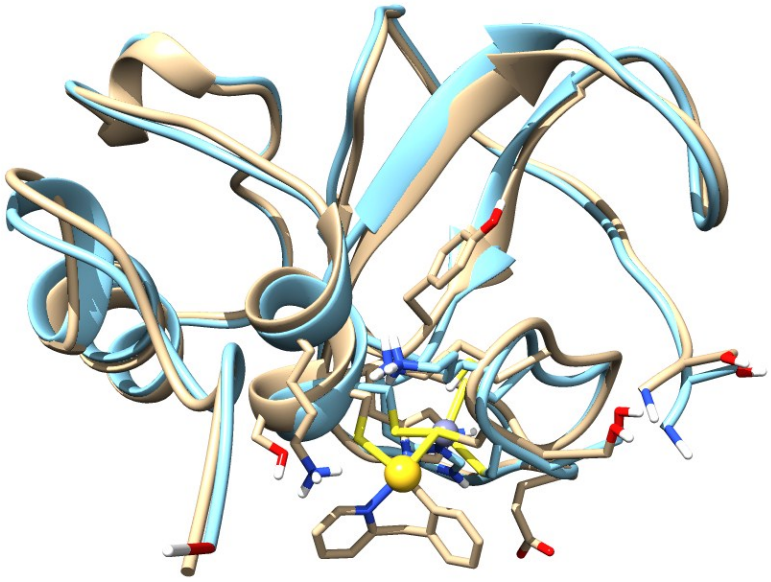

Figure S19. Superimposed structures of the most stable isomer of the complex between **Au-C^N** and the zinc-finger domain of PARP-1, whose geometry was fully optimized by QM/MM calculations.

10. References

[1] K. Palanichamy, A. C. Ontko, *Inorg. Chim. Acta* **2006**, *359*, 44-52.

[2] a) B. Bertrand, S. Spreckelmeyer, E. Bodio, F. Cocco, M. Picquet, P. Richard, P. Le Gendre, C. Orvig, M. A. Cinellu, A. Casini, *Dalton Trans.* **2015**, *44*, 11911-11918; b) M. A. Cinellu, A. Zucca, S. Stoccoro, G. Minghetti, M. Manassero, M. Sansoni, *J. Chem. Soc. Dalton Trans.* **1995**, 2865-2872.

[3] G. Marcon, S. Carotti, M. Coronnello, L. Messori, E. Mini, P. Orioli, T. Mazzei, M. A. Cinellu, G. Minghetti, *J. Med. Chem.* **2002**, *45*, 1672-1677.

[4] M. Nonoyama, K. Nakajima, K. Nonoyama, *Polyhedron* **1997**, *16*, 4039-4044.

[5] U. A. Laskay, C. Garino, Y. O. Tsybin, L. Salassa, A. Casini, *Chem. Comm.* **2015**, *51*, 1612-1615.

[6] A. de Almeida, A. F. Mosca, D. Wragg, M. Wenzel, P. Kavanagh, G. Barone, S. Leoni, G. Soveral, A. Casini, *Chem. Comm.* **2017**, *53*, 3830-3833.

[7] Y. Zhao, D. G. Truhlar, *J. Chem. Phys.* **2006**, *125*, 194101.

[8] P. J. Hay, W. R. Wadt, *J. Chem. Phys.* **1985**, *82*, 270-283.

[9] a) P. C. Hariharan, J. A. Pople, *Theor. Chim. Acta* **1973**, *28*, 213-222; b) M. M. Francl, W. J. Pietro, W. J. Hehre, J. S. Binkley, M. S. Gordon, D. J. DeFrees, J. A. Pople, *J. Chem. Phys.* **1982**, *77*, 3654-3665.

[10] J. Tomasi, B. Mennucci, R. Cammi, *Chem. Rev.* **2005**, *105*, 2999-3094.

[11] A. K. Rappe, C. J. Casewit, K. S. Colwell, W. A. Goddard, W. M. Skiff, *J. Am. Chem. Soc.* **1992**, *114*, 10024-10035.

[12] M. J. Frisch, G. W. Trucks, H. B. Schlegel, G. E. Scuseria, M. A. Robb, J. R. Cheeseman, G. Scalmani, V. Barone, G. A. Petersson, H. Nakatsuji, X. Li, M. Caricato, A. V. Marenich, J. Bloino, B. G. Janesko, R. Gomperts, B. Mennucci, H. P. Hratchian, J. V. Ortiz, A. F. Izmaylov, J. L. Sonnenberg, Williams, F. Ding, F. Lipparini, F. Egidi, J. Goings, B. Peng, A. Petrone, T. Henderson, D. Ranasinghe, V. G. Zakrzewski, J. Gao, N. Rega, G. Zheng, W. Liang, M. Hada, M. Ehara, K. Toyota, R. Fukuda, J. Hasegawa, M. Ishida, T. Nakajima, Y. Honda, O. Kitao, H. Nakai, T. Vreven, K. Throssell, J. A. Montgomery Jr., J. E. Peralta, F. Ogliaro, M. J. Bearpark, J. J. Heyd, E. N. Brothers, K. N. Kudin, V. N. Staroverov, T. A. Keith, R. Kobayashi, J. Normand, K. Raghavachari, A. P. Rendell, J. C. Burant, S. S. Iyengar, J. Tomasi, M. Cossi, J. M. Millam, M. Klene, C. Adamo, R. Cammi, J. W. Ochterski, R. L. Martin, K. Morokuma, O. Farkas, J. B. Foresman, D. J. Fox, Wallingford, CT, **2016**.